Environmental Science Nano



PAPER

View Article Online
View Journal | View Issue



Cite this: Environ. Sci.: Nano, 2021, 8, 795

Predicting the adsorption of organic pollutants on boron nitride nanosheets *via in silico* techniques: DFT computations and QSAR modeling†

Ya Wang,^a Weihao Tang,^b Yue Peng, ¹

ya Zhongfang Chen, ¹

to *c*

Jingwen Chen, ¹

** Zijun Xiao, ^b Xiaoguang Zhao, ^d Yakun Qu^d and Junhua Li ¹

** Li ¹

*

Investigating the adsorption of organic pollutants onto boron nitride nanosheets is crucial for designing novel boron nitride adsorbents so as to remove pollutants from the environment. In this study, we performed density functional theory (DFT) computations to investigate the adsorption of 28 aromatic compounds onto boron nitride nanosheets, and developed four quantitative structure–activity relationship (QSAR) models for predicting the logarithm of the adsorption equilibrium constant (log K) values of organic pollutants adsorbed onto boron nitride nanosheets in both gaseous and aqueous environments. The DFT-predicted adsorption energies showed that boron nitride nanosheets exhibit stronger adsorption capability than graphene. Our QSAR analyses revealed that van der Waals interactions play dominant roles in gaseous adsorption, while van der Waals and hydrophobic interactions are the main driving forces in aqueous adsorption. This work demonstrates that *in silico* QSAR models can serve as efficient tools for high-throughput prediction of log K values for organic pollutants adsorbed onto boron nitride nanomaterials.

Received 19th November 2020, Accepted 19th January 2021

DOI: 10.1039/d0en01145b

rsc.li/es-nano

Environmental significance

The superior physical chemical properties of boron nitride nanomaterials endow them with diverse promising applications in different fields. However, their applications as boron nitride adsorbents in removing organic pollutants from the environment is at a nascent stage. Investigating the adsorption behaviors of organic pollutants onto boron nitride nanomaterials and developing prediction models to obtain the adsorption data efficiently are crucial for designing novel adsorbents and extending their applications in the environment. Herein DFT computations were utilized for investigating the adsorption of 28 organic compounds onto the boron nitride nanosheet in both gaseous and aqueous environments. Furthermore, four QSAR models for predicting adsorption equilibrium constant values were established, which can serve as efficient tools for high-throughput screening of effective sorbents only *via* clicking a mouse.

1. Introduction

To date, more than 350 000 chemicals and their mixtures being registered have been produced and utilized, and new chemical products are entering the market with a rate of 12 000 per day.² These chemicals will be inevitably released into the environment during their lifecycle and become potential environmental pollutants, which give rise to adverse effects on human beings and the environment. Removing these pollutants from the environment is very important for protecting the health of ecosystems. Adsorption, due to its convenient operation, high efficiency, and low-energy consumption, has been extensively applied for eliminating or reducing pollutants from the environment.3-9 The hexagonal boron nitride nanosheet, as an analogue for graphene, has shown great potential in separating contaminants from the environment by adsorption due to its high specific surface area and chemical stability. 10-13 Therefore, exploring the adsorption

^a State Key Joint Laboratory of Environment Simulation and Pollution Control, School of Environment, Tsinghua University, Beijing 100084, China. E-mail: pengyue83@tsinghua.edu.cn

^b Key Laboratory of Industrial Ecology and Environmental Engineering (MOE), School of Environmental Science and Technology, Dalian University of Technology, Linggong Road 2, Dalian 116024, China. E-mail: jwchen@dlut.edu.cn

^c Department of Chemistry, University of Puerto Rico, San Juan, PR 00931, USA. E-mail: zhongfangchen@gmail.com

^d SINOPEC Research Institute of Petroleum Processing (RIPP), Beijing 100083, China

 $[\]dagger$ Electronic supplementary information (ESI) available: (1) Adsorption equilibrium configuration (Table S1); (2) charge transfer between the compound and the boron nitride nanosheet (Table S2); (3) estimated logarithm values for the adsorption equilibrium coefficient (log K) of fluorene (Table S3); (4) Williams plots of standardized residuals (δ^*) versus leverage values (h) for pp-LFER models (Fig. S1); (5) Williams plots of standardized residuals (δ^*) versus leverage values (h) for QSAR models (Fig. S2); (6) non-covalent interaction (NCI) analysis for the interactions between C6H6 and B $_{15}N_{15}H_{14}$ with the Multiwfn program (Fig. S3). See DOI: 10.1039/d0en01145b

of pollutants onto boron nitride nanomaterials is of great significance to develop novel boron nitride-based adsorbent materials for removing contaminants.

Previous experimental studies indicated that boron nitride nanomaterials have good adsorption capabilities towards various species such as metal ions, dyes, and organic solvents.3,7,14,15 Moreover, different adsorption mechanisms, e.g., van der Waals forces, π - π stacking and electrostatic interactions, may exist simultaneously during adsorption processes. However, the adsorption behavior of many organic pollutants, especially emerging pollutants (e.g., phthalate ester), onto boron nitride nanomaterials is still unclear, and the adsorption mechanism is not well understood.

Modern computational techniques provide us with an alternative method to investigate adsorption behaviors, which is more efficient than conventional experiments and can provide an atomic level of understanding. 16-20 Considering the large quantities of environmental contaminants, simulating their adsorption behavior towards boron nitride one by one is daunting, time-consuming, and costly, if not impossible. Therefore, it is essential to develop predictive models to obtain the adsorption data on boron nitride nanomaterials.

Very recent studies demonstrated the powerful ability of quantitative structure-activity relationships (QSARs) in predicting the adsorption of organic pollutants on carbon nanomaterials. 18,21-25 In these QSAR models, the most important input parameters are the Abraham descriptors for polyparameter linear free energy relationships (pp-LFERs), which are determined experimentally, and the descriptors characterizing the molecular structures, which can be obtained by theoretical calculations. However, no QSAR model has been proposed to predict the adsorption of organic pollutants onto boron nitride nanomaterials so far.

In this work, we theoretically investigated the adsorption of 28 different aromatic compounds (including phthalate esters) on boron nitride nanosheets in both gaseous and aqueous phases by means of density functional theory (DFT) computations. Based on the DFT computational results, the logarithm of the adsorption equilibrium coefficient $(\log K)$ was estimated. In combination with the Abraham descriptors for these 28 compounds, we established pp-LFER models for gaseous and aqueous phases, and evaluated the contributions from different adsorption mechanisms. Furthermore, by utilizing the theoretical molecular structure descriptors, we developed two QSAR models which can predict the adsorption of emerging pollutants in the application domain (AD) whose Abraham descriptors are not available. The QSAR models established in this study not only can offer insights into the adsorption mechanisms of boron nitride nanomaterials, but also lay a foundation for further development of theoretical prediction models to estimate adsorptions onto boron nitride nanomaterials.

2. Computational details

2.1. Organic compounds and boron nitride nanosheets

Herein, 28 aromatic compounds (Table 1) with diverse functional groups, i.e., -NO2, -CH3, -OH, -NH2, -CH2OH, -CH₂CH₃, -C(O)CH₃, -CH₂CH₂OH, -C(O)OCH₃, -OC(O)CH₃, -CH2CH2CH3, -C(O)OCH2CH3 and -C6H5, are used as adsorbate models; a boron nitride nanosheet with a supercell size of 8 × 8 × 1 (containing 64 boron atoms and 64 nitrogen atoms) is employed as the adsorbent model.

2.2. Density functional theory computations

All the computations were performed in the frame of density functional theory (DFT) by the DMol3 program.26,27 The Perdew-Burke-Ernzerhof (PBE) functional within the generalized gradient approximation was employed to describe the exchange and correlation potentials.28 The chosen basis set was a double-numerical basis set with polarization functions (DNP), 29,30 which is comparable to Gaussian 6-31G(d,p).31 Besides, the PBE + D2 method with the Grimme van der Waals (vdW) correction³² was used for 1 Monkhorst-Pack k-point mesh was utilized, and a

Table 1 Organic compounds and estimated logarithm values for the adsorption equilibrium coefficient (log K) from our DFT computations in gaseous and aqueous environments

			$\log K$ (DFT)	
			Gaseous	Aqueous
No.	Compound	Substituents	phase	phase
1	Benzene		2.50	1.61
2	Nitrobenzene	$-NO_2$	3.31	3.81
3	Toluene	-CH ₃	4.35	5.04
4	Phenol	-OH	5.06	1.47
5	Aniline	$-NH_2$	4.44	2.45
6	1,3-Dinitrobenzene	$-NO_2$	5.11	3.70
7	4-Nitrotoluene	$-NO_2$, $-CH_3$	5.32	4.54
8	2, 4-Dinitrotoluene	$-NO_2$, $-CH_3$	8.90	7.42
9	Anthracene		11.43	13.69
10	Pyrene		12.04	13.95
11	Biphenyl		11.00	7.76
12	3,5-Dimethylphenol	-CH ₃ , -OH	9.22	6.01
13	Ethylbenzoate	-C(O)OCH ₂ CH ₃	8.77	7.55
14	4-Ethylphenol	-CH ₂ CH ₃ , -OH	7.28	6.03
15	Methylbenzoate	-C(O)OCH ₃	6.88	5.66
16	(3-Methylphenyl)	-CH ₃ , -CH ₂ OH	6.11	4.68
	methanol			
17	1-Methylnaphthalene	-CH ₃	9.66	9.04
18	Phenylacetate	-OC(O)CH ₃	4.44	1.95
19	2-Phenylethanol	-CH ₂ CH ₂ OH	5.28	5.03
20	Phenylmethanol	-CH ₂ OH	3.71	3.85
21	Propylbenzene	-CH ₂ CH ₂ CH ₃	9.10	4.68
22	<i>p</i> -Xylene	-CH ₃	6.17	4.34
23	Dimethyl phthalate	-C(O)OCH ₃	8.27	6.18
	(DMP)			
24	Diethyl phthalate (DEP)	-C(O)OCH ₂ CH ₃	10.51	9.71
25	Acetophenone	-C(O)CH ₃	5.47	2.83
26	Naphthalene	-(-)3	7.36	6.34
		NO		
27	1,2-Dinitrobenzene	$-NO_2$	5.13	4.69

Methfessel-Paxton smearing of 0.005 Ha (ref. 33) was employed for the Brillouin-zone integration. The popular conductor-like screening model (COSMO)³⁴ with the dielectric constant (78.54) for water was used to implicitly simulate the aqueous environment. COSMO is superior to many other solvent reaction field methods. In this model, the surface charges of a cavity having the same shape as the solute molecule, which describe the electrostatic interactions between the solvent and solute, are determined with the electrostatic potentials directly.³⁵

In order to simulate the adsorption onto a boron nitride nanosheet, first the adsorbate models (28 aromatic compounds) and the adsorbent model (a BN nanosheet) were optimized respectively. Afterwards, the global minimum sorbate locations for the 28 complex systems (each including one compound adsorbed on the BN nanosheet) were searched by using the sorption module of Materials Studio 8.0. The most stable configurations obtained were further optimized with the aforementioned DFT method.

2.3. Estimation for the adsorption equilibrium coefficient (K)

The changes of Gibbs free energy (ΔG) during the adsorption process can be estimated from the changes of total energy (ΔE), zero point energy (ΔZ PE), and entropy (ΔS) following the equation:

$$\Delta G = \Delta E + \Delta Z P E - T \Delta S \tag{1}$$

where T is temperature, and T = 298.15 K is used for all the calculations. ΔE is also the adsorption energy of a specific adsorbate on the BN nanosheet. ΔE , ΔZPE and ΔS can be obtained using the following equations:

$$\Delta E = E_{\rm BN+X} - E_{\rm X} - E_{\rm BN} \tag{2}$$

$$\Delta ZPE = ZPE_{BN+X} - ZPE_{X} - ZPE_{BN}$$
 (3)

$$\Delta S = S_{\rm BN+X} - S_{\rm X} - S_{\rm BN} \tag{4}$$

where the subscript BN stands for the boron nitride nanosheet, X represents the adsorbate, while BN + X denotes the complex system including the boron nitride nanosheet and the adsorbed compound. The total energies ($E_{\rm BN+X}$, $E_{\rm X}$ and $E_{\rm BN}$), zero-point energies ($ZPE_{\rm BN+X}$, $ZPE_{\rm X}$ and $ZPE_{\rm BN}$), and entropies ($S_{\rm BN+X}$, $S_{\rm X}$ and $S_{\rm BN}$) were obtained by DFT computations.

We further calculated the adsorption equilibrium coefficient (K) with ΔG .

$$K = e^{-\frac{\Delta G}{RT}} \tag{5}$$

where K is unitless; R is the universal gas constant, *i.e.*, 8.314 J mol⁻¹ K⁻¹. The calculated K is equivalent to the experimentally determined K, which is defined as

$$K = q_{\rm e}/C_{\rm e} \tag{6}$$

where q_e represents the equilibrium concentration of the compounds on boron nitride nanosheets; C_e denotes the equilibrium concentration of the compounds in aqueous/gaseous environments.

2.4. Molecular structure descriptors

Note that the adsorption of organic pollutants on boron nitride nanomaterials is assumed to be governed by different specific and nonspecific interactions.^{3,36} Abraham descriptors can characterize these diverse molecular interactions, and are widely utilized in pp-LFERs, which have the following forms (eqn (7) is used for the partitioning within two condensed phases; while eqn (8) is applied for the partitioning between condensed and gas phases.),^{37–43}

$$\log K = eE + sS + aA + bB + \nu V + c \tag{7}$$

$$\log K = eE + sS + aA + bB + lL + c \tag{8}$$

The three dimensional (3D) molecular structures of the 28 compounds were obtained by geometry optimization by DFT, and confirmed to be the local minima by frequency analyses. With these optimized molecular structures, we obtained 4885 theoretical molecular structure descriptor values by using the Dragon software (Ver. 6.0).⁴⁸ After deleting the descriptors with constant and near-constant values, and selecting the descriptors characterizing the property of molecules which may influence the adsorption, we chose 108 theoretical descriptors to establish QSAR models.

2.5. QSAR model development and evaluation

These 28 compounds were randomly split into a training set consisting of 24 compounds and a validation set including 4 compounds. Based on the $\log K$ values of DFT calculations and the molecular structure descriptor values for the training set, we utilized the multiple linear regression (MLR) analysis in the SPSS (SPSS 22.0) software package to build up QSAR models, including pp-LFER models for which Abraham descriptors are used as input variables and the models for which Dragon descriptors are input variables. Furthermore,

the determination coefficient (R^2) , root mean square error for the training set (RMSE_t) and for the validation set (RMSE_v), leave-one-out cross-validated Q^2 (Q^2_{LOO}) and external explained variance $(Q_{\rm V}^2)$ were calculated for assessing the goodness of fit, robustness, and prediction ability of QSAR models. Moreover, the application domains (ADs) for the predictive models were characterized by Williams plots using standardized residuals (δ^*) and leverage values (h_i).⁴⁹

3. Results and discussion

3.1. log K values of DFT calculations and adsorption energies on boron nitride nanosheets

Table 1 lists the log K values of 28 aromatic compounds adsorbed on BN nanosheets in the gaseous and aqueous environments predicted by our DFT computations. The predicted $\log K$ value of benzene on the boron nitride nanosheet in the gaseous phase is 2.50, which is comparable with the experimentally measured value, 2.88.50 We also estimated the $\log K$ value of nitrobenzene onto graphene in the aqueous phase for which the experimental value is available, and found that the predicted value (4.96) is in good agreement with the experimental one (5.31).⁵¹ These comparisons show that DFT computations can well reproduce the experimental adsorption data, and can be used to obtain adsorption data when the experimental values are not available.

In addition, all the optimized equilibrium configurations are summarized in Table S1 (ESI†). The benzene rings for the 28 organic compounds are all parallel to the boron nitride nanosheet (Table S1†). The distances between the mass center of these molecules and the BN nanosheet plane are in the range of 3.168-3.680 Å, implying the existence of van der Waals interactions. Besides, we performed Hirshfeld population analysis for each compound's adsorption on the BN nanosheet (Table S2†), and the small charge transfer (-0.064-0.016 e in the gaseous phase and -0.096-0.023 e in the aqueous phase) from the compound to the BN nanosheet also indicates physisorption.

We further compared the adsorption energies of 18 different organic compounds onto BN nanosheets with the corresponding values on graphene, in order to examine the differences in adsorption capability between boron nitride and carbon nanomaterials. As shown in Table 2 and Fig. 1, the adsorption energies for these 18 aromatic compounds on BN nanosheets are stronger than those on graphene both in gaseous and aqueous environments, and the adsorption energies on graphene correlate with those on the boron nitride nanosheet significantly (Fig. 1). Based on these DFT results, the boron nitride nanosheet possibly performs better than graphene in removing contaminants by adsorption.

3.2. QSAR models with Abraham descriptors for $\log K$ values on boron nitride

Based on the Abraham descriptors for the 28 organic compounds, we built up and validated the following pp-LFER predictive models, for the gaseous environment,

$$\log K = -2.508 - 2.352 \times E - 5.510 \times S + 2.509 \times A - 4.252 \times B + 3.670 \times L$$
 (9)

$$n_{\rm t}$$
 = 24, R^2 = 0.89, RMSE_t = 0.89, F = 29.73, p < 0.001,

$$n_{\rm v} = 4$$
, $Q_{\rm LOO}^2 = 0.89$, $Q_{\rm V}^2 = 0.99$, RMSE_V = 1.88

for the aqueous environment,

$$\log K = -5.578 + 3.135 \times E - 2.184 \times S + 0.673 \times A - 1.431 \times B + 9.879 \times V$$
 (10)

$$n_t = 24$$
, $R^2 = 0.90$, RMSE_t = 0.99, $F = 34.12$, $p < 0.001$,

Table 2 Adsorption energies (ΔΕ) for 18 aromatic compounds on the boron nitride nanosheet and graphene in gaseous and aqueous environments

		Gaseous		Aqueous		
No.	Name	ΔE _BN (kcal mol ⁻¹)	$\Delta E_{\rm G}^{24}$ (kcal mol ⁻¹)	ΔE _BN (kcal mol ⁻¹)	$\Delta E_{\rm G}^{24}$ (kcal mol ⁻¹)	
1	Benzene	-17.1	-12.9	-15.9	-11.8	
2	Nitrobenzene	-21.2	-16.2	-19.7	-14.3	
3	Toluene	-19.2	-15.3	-19.2	-13.0	
4	Phenol	-19.2	-14.5	-16.6	-12.4	
5	Aniline	-21.2	-14.9	-18.1	-12.0	
6	Phenylmethanol	-19.4	-15.4	-19.8	-14.1	
7	Phenylacetate	-20.8	-15.5	-18.2	-12.5	
8	Methylbenzoate	-24.4	-19.3	-22.5	-17.0	
9	Ethylbenzoate	-27.2	-21.3	-25.0	-18.8	
10	Acetophenone	-23.8	-18.5	-20.9	-15.6	
11	1,3-Dinitrobenzene	-24.1	-20.0	-21.5	-17.5	
12	1,2-Dinitrobenzene	-22.4	-17.6	-20.5	-15.4	
13	4-Nitrotoluene	-23.9	-19.5	-22.8	-17.5	
14	Biphenyl	-29.3	-22.0	-26.6	-20.7	
15	Naphthalene	-25.0	-18.8	-23.9	-18.0	
16	Phenanthrene	-32.9	-26.6	-31.3	-25.1	
17	Anthracene	-33.1	-26.9	-32.7	-25.3	
18	Pyrene	-36.0	-30.5	-35.1	-27.0	

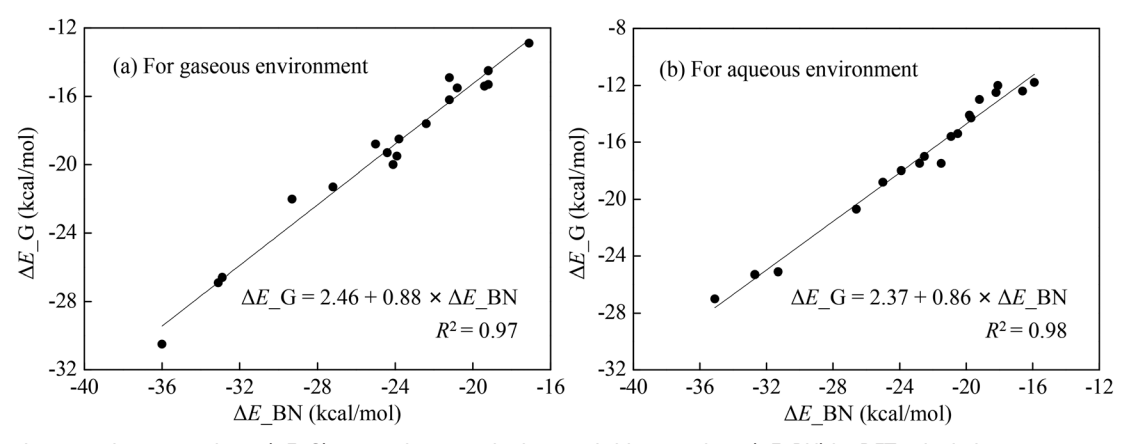


Fig. 1 Adsorption energies on graphene (ΔE _G) versus those on the boron nitride nanosheet (ΔE _BN) by DFT calculations.

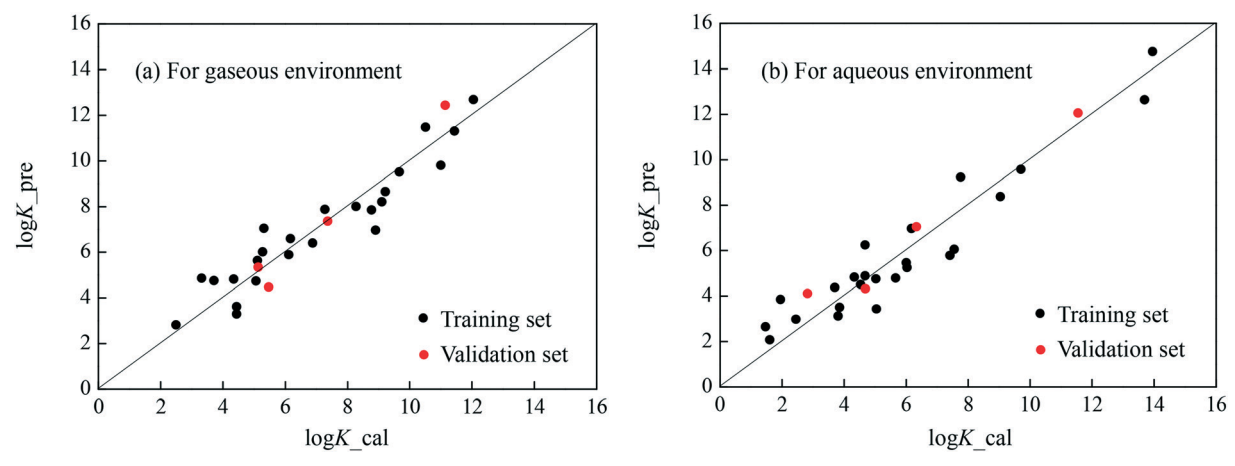


Fig. 2 Predicted $\log K$ values with pp-LFER models ($\log K_{pre}$) versus those calculated by the DFT method ($\log K_{cal}$).

$$n_{\rm v} = 4$$
, $Q_{\rm LOO}^2 = 0.83$, $Q_{\rm V}^2 = 0.94$, RMSE_V = 0.80

where n_t is the number of compounds in the training set, and $n_{\rm v}$ denotes the number of compounds in the validation set. The values for R^2 , Q_V^2 , Q_{LOO}^2 , RMSE_t and RMSE_V imply that these two pp-LFER models have satisfactory goodness of fit, robustness and prediction ability, as they comply with the criteria $(R^2 >$ 0.60 and $Q^2 > 0.50$) proposed by Golbraikh et al.⁵²

Fig. 2 shows that the predicted log K values from the pp-LFER models agree well with the calculated log K values via the DFT method. Note that for the emerging pollutants phthalate esters, i.e., DMP and DEP in the current study, their predicted $\log K$ values [8.00 (DMP_gaseous), (DMP_aqueous), 11.48 (DEP_gaseous) 9.57 (DEP_aqueous)] from the pp-LFER models are also comparable with the calculated ones [8.27 (DMP_gaseous), 6.18 (DMP_aqueous), 10.51 (DEP_gaseous) and (DEP_aqueous)] from DFT computational results. In terms of the application of the two pp-LFER models, besides the four compounds in the validation set (i.e., acetophenone, naphthalene, 1, 2-dinitrobenzene, and phenanthrene), we also predicted the $\log K$ value for a compound outside the

dataset, namely fluorene. The predicted log K values from the models are comparable with those estimated with the DFT method (Table S3†). All of these demonstrate that these two pp-LFER models can effectively offer adsorption data for organic pollutants including phthalate esters towards boron nitride nanosheets in both gaseous and aqueous environments, and thus can serve as a high-throughput prediction tool.

As displayed in Fig. S1,† all the standardized residuals for the compounds in the training set comply with the criteria $|\delta^*|$ <3, indicating that there are no outliers. These two pp-LFER models (eqn (9) and (10)) can predict the adsorption towards boron nitride nanosheets for diverse organic i.e., benzene, phenols, nitrobenzenes, alkylbenzenes, anilines, alcohols, esters, ketones, biphenyls and polycyclic aromatic hydrocarbons (PAHs). In terms of the functional groups, the application domain covers various compounds with different functional groups including -NO2, -CH₃, -OH, -NH₂, -CH₂OH, -CH₂CH₃, -OC(O)CH₃, -C(O) CH_3 , $-C(O)OCH_3$, $-CH_2CH_2OH$, $-CH_2CH_2CH_3$ and -C(O)OCH₂CH₃. When a compound is outside the application domain of the developed models, its prediction is unreliable.

3.3. QSAR models with Dragon descriptors for $\log K$ values on boron nitride

Note that Abraham descriptor values depend on experimental determinations, and the number of compounds having Abraham descriptor values is ca. 3700.47 For some of the organic compounds lacking Abraham descriptor values, if they locate in the application domain of previous models, 53,54 their Abraham descriptor values can be estimated. However, the accuracy of the predicted descriptor values is inferior to those derived from experimental data. Meanwhile for many organic compounds outside the application domain, the predicted Abraham descriptor values for these compounds are unreliable. Therefore, it is of great importance to develop QSAR models with only theoretical molecular structure descriptors which can be calculated by computational software directly.

Herein, the optimal QSAR models with Dragon descriptors for predicting the adsorption of organic compounds onto boron nitride nanosheets were developed: for the gaseous environment,

$$\log K = -6.950 + 1.318 \times Sv + 1.323 \times nArOH - 2.058$$
$$\times B05[C-O] - 0.365 \times F05[C-C]$$
(11)

$$n_{\rm t} = 24$$
, $R^2 = 0.91$, RMSE_t = 0.82, $F = 47.175$, $p < 0.001$,

$$n_{\rm v}=4,~Q_{\rm LOO}^2=0.87,~Q_{\rm V}^2=0.94,~{\rm RMSE_{\rm V}}=0.72$$

for the aqueous environment,

$$\log K = -2.788 + 1.247 \times nC - 2.210 \times NRS + 1.193 \times nArNO_2$$

$$-1.009 \times H-051$$
(12)

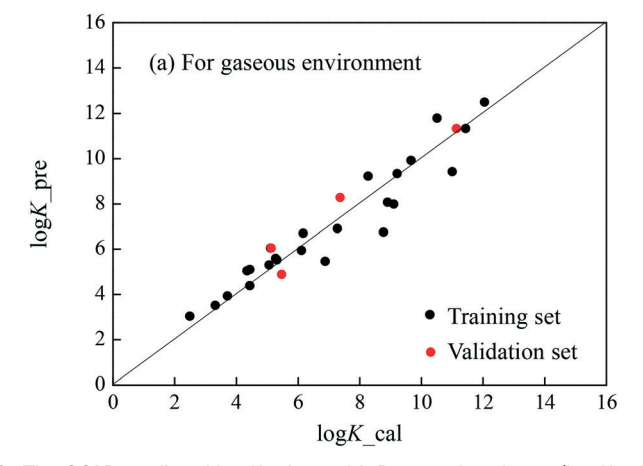
$$n_{\rm t} = 24$$
, $R^2 = 0.93$, RMSE_t = 0.88, $F = 58.75$, $p < 0.001$,

$$n_{\rm v} = 4$$
, $Q_{\rm LOO}^2 = 0.82$, $Q_{\rm V}^2 = 0.98$, RMSE_V = 0.85

Likewise, these two QSAR models with $R^2 > 0.60$ and Q^2 $(Q_{LOO}^2 \text{ and } Q_V^2) > 0.50 \text{ have high goodness of fit, robustness}$ and prediction ability. All the values of variable inflation factors (VIFs) for the descriptors utilized in eqn (10) and (11) are less than 10, which implies that there is no serious multicollinearity among these variables.55

As shown in Fig. 3, the predicted $\log K$ values by the QSAR models with Dragon descriptors (eqn (11) and (12)) are in good agreement with those from DFT estimation. For the gaseous phase, in comparison with the pp-LFER model (eqn (9)), the QSAR model (eqn (11)) has fewer descriptors and better goodness of fit, robustness and prediction ability. For the aqueous phase, the QSAR model (eqn (12)) using fewer descriptors has better goodness of fit, while the pp-LFER model (eqn (10)) has a lower RMSE_v value and comparable robustness. In terms of the prediction accuracy for the phthalate esters, the pp-LFER models (eqn (9) and (10)) perform better than the QSAR models (eqn (11) and (12)), since the average prediction errors for phthalate esters with the pp-LFER models [0.62 (gaseous phase) and 0.47 (aqueous phase)] are less than those with the QSAR models [1.12 (gaseous phase) and 0.78 (aqueous phase)]. We also applied these two QSAR models for predicting the $\log K$ values for fluorene (Table S3†). These results showed that the predicted log K values for fluorene with the pp-LFER models (eqn (9) and (10)) are closer to those from DFT calculations than those predicted with the QSAR models (eqn (11) and (12)).

Besides, based on the standardized residuals (δ^*) and leverage values (h) for the compounds in the training set, we characterized the application domains (ADs) as illustrated in Fig. S2.† With the $|\delta^*|$ values less than three, all the compounds are located in the ADs. Note that the h value for 4-ethylphenol (1.0) is larger than the warning leverage value $(h^* = 0.625)$ while its $|\delta^*|$ value is smaller than 3 (Fig. S2b†), indicating that its structure is very different from the other compounds in the training set and it is influential on the prediction model for the aqueous phase. It is known that the application domain for a prediction model depends on the compounds utilized when this model is developed. The established QSAR models (eqn (11) and (12)) with the Dragon descriptors have the same ADs with those for the pp-LFERs



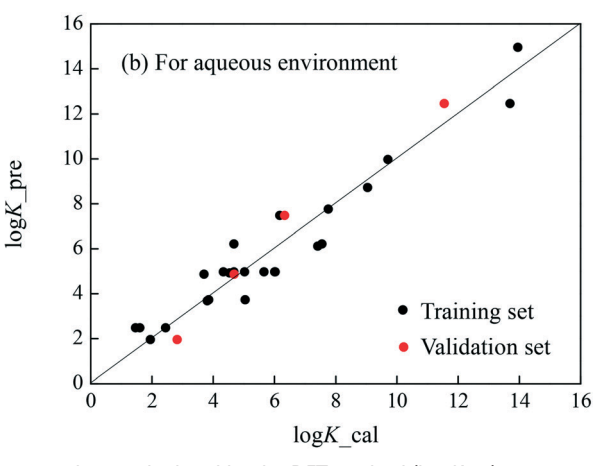


Fig. 3 The QSAR predicted $\log K$ values with Dragon descriptors ($\log K_{pre}$) versus those calculated by the DFT method ($\log K_{cal}$).

(eqn (9) and (10)), covering diverse organic compounds. Moreover, the two models (eqn (11) and (12)) can be applied for obtaining $\log K$ values of more emerging pollutants lacking pp-LFER descriptor values.

3.4. Adsorption mechanisms

pp-LFER models. As shown in the developed pp-LFER models (eqn (9) and (10)), for both gaseous and aqueous systems, the five sets of parameters, namely eE, vV/lL, aA, bB and sS, are used, but they have different values, which indicate that the molecular interactions they are describing play different roles in the adsorption (Fig. 4).

In terms of the adsorption in the gaseous environment, the term *lL* plays a dominant role as its relative contribution to the adsorption ranges from 53% to 68%. lL in eqn (8) represents dispersion interactions. Therefore, the dispersion interactions are key driving forces for adsorption on the BN nanosheet in the gaseous phase. The relative contribution to the adsorption for sS is in the range of 12-25%, which is second only to that for *LL*. The term sS describes the interactions related to the polarity and polarizability of the adsorbates. Note that the fitting coefficient s is negative, implying that the compound having a high value of S is not liable to be adsorbed onto boron nitride nanosheets. As shown in eqn (9) and Fig. 4, the H-bonding interactions between the H-donating adsorbate and H-accepting adsorbent, characterized by the term aA, do positively contribute (ca. 0-6%) to the adsorption. Meanwhile for the H-bonding interactions between the H-accepting adsorbate and H-donating adsorbent, being denoted by the term bB, its contribution to the adsorption ranges from 2% to 10% negatively. The reason may be that the nitrogen atoms on the boron nitride nanosheet are rich in electrons, which can accept hydrogen atoms from the compounds lacking electrons, thereby increasing the interactions between the compounds and the nanosheet. In addition, the term eE representing the interactions related to the π or n-electron pair has a negative

contribution (ranging from 4% to 13%) to the adsorption. It implies that the compound possessing fewer π or n electrons tends to be adsorbed by boron nitride nanomaterials for accepting the electrons.

For the adsorption in the aqueous environment, the term vV representing the dispersion and hydrophobic interactions has the most significant influence on the log K values with relative contributions ranging from 41% to 59%, which indicates that the dispersion and hydrophobic interactions play vital roles in the adsorption of organic compounds onto the boron nitride nanosheet. The term eE, denoting the interactions related to the π or n-electron pair, has a positive contribution to the adsorption with the relative contribution in the range of 8-26%. Note that its contribution in the aqueous phase is positive, which is contrary to that in the gaseous phase, most likely the π or n electrons from the compound can interact with one hydrogen atom in water molecules, and the other hydrogen atom in water molecules can interact with the nitrogen atoms of the boron nitride surface, thereby assisting the adsorption of the compound towards boron nitride nanosheets. Therefore, it seems that the compound having more π or n electrons becomes liable to be adsorbed towards the boron nitride nanosheet in the aqueous phase. sS represents the interactions related to the polarity and polarizability of the compounds, and has a negative contribution (ranging from 5-15%) to the adsorption. Besides, hydrogen bonding interactions also play roles in the adsorption. The term aA describing the H-bonding interactions between the H-donating adsorbate and H-accepting system (including the adsorbent and water) contributes positively to the adsorption (ranging from 0-2%), while the term bB representing the H-bonding interactions between the H-accepting adsorbate and H-donating system contributes negatively to the adsorption (in the range of 1-5%). The roles for hydrogen donating/accepting abilities in the adsorption on boron nitride nanosheets in the aqueous phase are similar to those in the gaseous phase.

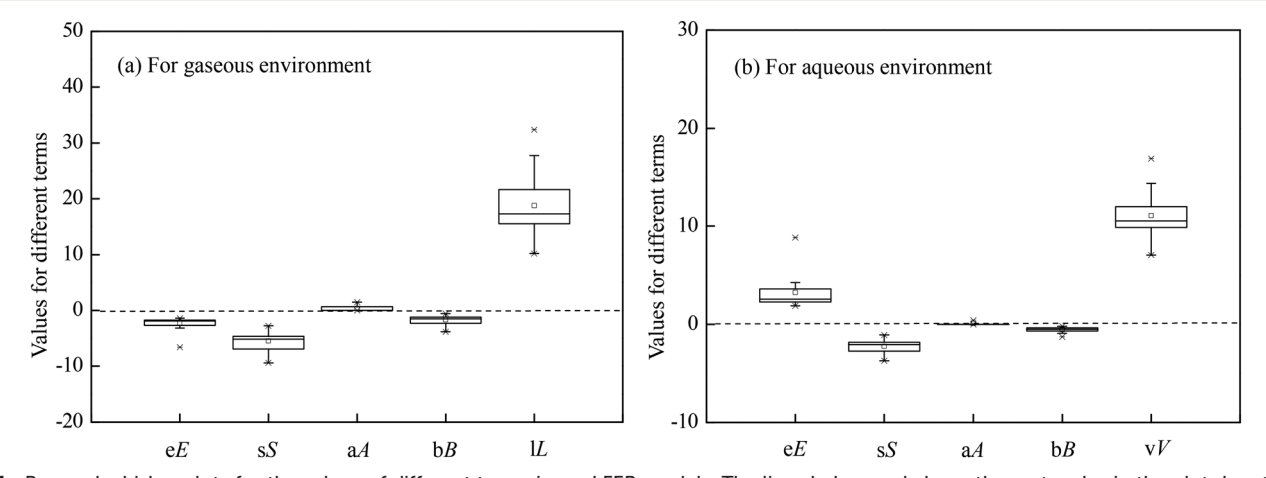


Fig. 4 Box and whisker plots for the values of different terms in pp-LFER models. The lines below and above the rectangles in the plot denote the minimum and maximum values for each term; the lines within the rectangles mean the 50th percentiles; the bottom and the top for the rectangles represent the 25th and 75th percentiles.

Table 3 Description for the predictive variables and their standardized coefficients, t, p values and variable inflation factor (VIF)

Gaseous phase					
Descriptors	Description	Standardized coefficients	t^a	p^a	VIF
Sv	Sum of atomic van der Waals volumes (scaled on the carbon atom)	1.403	7.275	< 0.001	7.724
<i>n</i> ArOH	Number of aromatic hydroxyls	0.161	2.194	< 0.05	1.115
B05[C-O]	Presence/absence of C–O at topological distance 5	-0.377	-4.413	< 0.001	1.513
F05[C-C]	Frequency of C–C at topological distance 5	-0.523	-2.634	< 0.02	8.189

Descriptors	Description	Standardized coefficients	t^a	p^a	VIF
nC	Number of carbon atoms	1.011	14.572	< 0.001	1.222
NRS	Number of ring systems	-0.138	-2.114	< 0.05	1.080
$nArNO_2$	Number of nitro groups (aromatic)	0.222	3.296	< 0.01	1.149
H-051	H attached to alpha-C	-0.189	-2.987	< 0.01	1.016

^a t denotes the statistic from the t-test; p is the significance level of the t-test.

QSAR models with Dragon descriptors. Table 3 lists the predictive variables and their standardized coefficients, t, pvalues, and variable inflation factor (VIF) for the QSAR models with Dragon descriptors (eqn (11) and (12)). Note that the predictive variables used for the gaseous and aqueous phases are different, which implies that the adsorption mechanisms in the gaseous phase are different from those in the aqueous phase.

For the adsorption in the gaseous phase, as shown in eqn (11), the descriptors Sv, nArOH, B05[C-O] and F05[C-C] are combined to predict the $\log K$ values. Sv, the sum of atomic van der Waals volumes (scaled on the carbon atom),⁵⁶ has the highest standardized coefficient among these four descriptors (Table 3), indicating that it is the most influential predictive variable for the adsorption onto the boron nitride nanosheet in the gaseous environment. It also indicates that van der Waals interactions play an important role in the adsorption, which is in good agreement with the pp-LFER model in the gaseous phase. Besides, the descriptor nArOH is the number of aromatic hydroxyls,57 and its coefficient is positive, which suggests that the compound having a large nArOH value tends to be adsorbed onto the boron nitride nanosheet, because the hydrogen atom from the aromatic hydroxyls lacking electrons can be liable to interact with the nitrogen atom possessing rich electrons from the boron nitride surface. The descriptors B05[C-O]58 and F05[C-C]59 denote different atom pairs, and both of them have negative coefficients. These two descriptors, to some extent, reflect the spatial structure of the compound. There exists steric hindrance during the adsorption for the compound having large values for B05[C-O] or F05[C-C].

When the adsorption in the aqueous phase is concerned, as illustrated in eqn (12), the descriptors, namely nC, NRS, $nArNO_2$ and H-051, contribute differently to the log K values. The standardized coefficients in Table 3 show that the descriptor nC (the number of carbon atoms)⁶⁰ is the most influential variable in predicting the $\log K$ values. The positive coefficient of nC indicates that the compound with more carbon atoms tends to be adsorbed on the boron nitride nanosheet. The descriptor nArNO2 (ref. 61) denoting the number of nitro groups (aromatic) has a positive coefficient, which indicates that when interacting with the boron nitride nanosheet, a compound with more nitro groups (aromatic) will have stronger interactions compared with a compound with fewer nitro groups (aromatic). This phenomenon can be understood by the electrophilic property of the nitro groups, which tend to withdraw the electrons from the surface of boron nitride, thereby increasing the interactions between the compounds and the boron nitride nanosheet. The descriptor H-051 is an atom-centered fragment, describing the existence of hydrogen attached to alpha-C.62 NRS characterizes the number of ring systems.⁶³ The coefficients for H-051 and NRS are both negative, implying that the compound with a lower H-051 or NRS value will be adsorbed by the boron nitride nanomaterial more easily.

Furthermore, taking benzene as an example, we computed its adsorption energy onto the boron nitride nanosheet without vdW correction, and found that the absolute values for the obtained adsorption energies without vdW corrections (7.2 kcal mol⁻¹ in the gaseous phase and 6.3 kcal mol⁻¹ in the aqueous phase) are ca. 10 kcal mol⁻¹ less than those (17.1 kcal mol⁻¹ in the gaseous phase and 15.9 kcal mol⁻¹ in the aqueous phase) calculated with the PBE + D2 method. It implies that the noncovalent interactions (van der Waals in particular) play significant roles in the adsorption, which is also supported by the non-covalent interaction analysis of the simplified model system (Fig. S3†).64

To summarize, the adsorption mechanisms of organic pollutants onto boron nitride nanosheets in the gaseous environment are different from those in the aqueous environment. The van der Waals interactions prevail in gaseous adsorption, while for aqueous adsorption, the main driving forces are van der Waals and hydrophobic interactions.

4. Conclusions

In this study, DFT computations were successfully utilized to probe the atomic-level details for adsorption of 28 diverse

organic compounds onto the boron nitride nanosheet in both gaseous and aqueous environments. Adsorption energies implied that the boron nitride nanosheet has stronger adsorption capability than graphene. Four QSAR models for predicting $\log K$ values were further established, which can serve as efficient tools for high-throughput screening of effective sorbents. In particular, when the pp-LFER descriptors of organic compounds are not available, the adsorption behavior can still be well predicted by the QSAR models with only theoretical molecular descriptors. Moreover, the developed QSAR models can provide us with insights into the mechanisms involved in the adsorption onto boron nitride nanomaterials. These in silico techniques, i.e., DFT computations and QSAR modeling, make it possible for us to obtain the adsorption data on boron nitride nanosheets only via clicking a mouse, and such techniques can be extended to many other sorbent systems.

Author contributions

The manuscript was written through contributions of all the authors. All the authors have given approval to the final version of the manuscript.

Conflicts of interest

The authors declare no competing financial interest.

Acknowledgements

This study was supported in China by the National Key Research and Development Program (2018YFC0214106 and 2017YFC0211000) and in USA by NASA (Grant Number 80NSSC19M0236) and the NSF Centre for the Advancement of Wearable Technologies (Grant 1849243).

References

- 1 Z. Wang, G. W. Walker, D. C. G. Muir and K. Nagatani-Yoshida, Toward a global understanding of chemical pollution: A first comprehensive analysis of national and regional chemical inventories, Environ. Sci. Technol., 2020, 54(5), 2575-2584.
- 2 S. Rojas and P. Horcajada, Metal-organic frameworks for the removal of emerging organic contaminants in water, Chem. Rev., 2020, 120(16), 8378-8415.
- 3 S. Yu, X. Wang, H. Pang, R. Zhang, W. Song, D. Fu, T. Hayat and X. Wang, Boron nitride-based materials for the removal of pollutants from aqueous solutions: A review, Chem. Eng. J., 2018, **333**, 343-360.
- 4 J. Zhao, Z. Y. Wang, J. White and B. S. Xing, Graphene in the aquatic environment: Adsorption, dispersion, toxicity and transformation, Environ. Sci. Technol., 2014, 48(17), 9995-10009.
- 5 Y. M. Xue, P. C. Dai, X. F. Jiang, X. B. Wang, C. Zhang, D. M. Tang, Q. H. Weng, X. Wang, A. Pakdel, C. C. Tang, Y. Bando and D. Golberg, Template-free synthesis of boron nitride

- foam-like porous monoliths and their high-end applications in water purification, J. Mater. Chem. A, 2016, 4, 1469-1478.
- 6 G. Lian, X. Zhang, S. Zhang, D. Liu, D. Cui and Q. Wang, Controlled fabrication of ultrathin-shell BN hollow spheres with excellent performance in hydrogen storage and wastewater treatment, Energy Environ. Sci., 2012, 5, 7072-7080.
- 7 D. Liu, W. Lei, S. Qin, K. Klika and Y. Chen, Superior adsorption of pharmaceutical molecules by highly porous BN nanosheets, Phys. Chem. Chem. Phys., 2016, 18, 84-88.
- 8 L. Jiang, Y. Liu, S. Liu, G. Zeng, X. Hu, X. Hu, Z. Guo, X. Tan, L. Wang and Z. Wu, Adsorption of estrogen contaminants by graphene nanomaterials under natural organic matter preloading: Comparison to carbon nanotube, biochar, and activated carbon, Environ. Sci. Technol., 2017, 51(11), 6352-6359.
- 9 J. Wang, B. Chen and B. S. Xing, Wrinkles and folds of activated graphene nanosheets as fast and efficient adsorptive sites for hydrophobic organic contaminants, Environ. Sci. Technol., 2016, 50(7), 3798-3808.
- 10 D. Golberg, Y. Bando, Y. Huang, T. Terao, M. Mitome, C. C. Tang and C. Y. Zhi, Boron nitride nanotubes and nanosheets, ACS Nano, 2010, 4, 2979-2993.
- 11 J. Ye, X. Zhu, B. Cheng, J. Yu and C. Jiang, Few-layered graphene-like boron nitride: A highly efficient adsorbent for indoor formaldehyde removal, Environ. Sci. Technol. Lett., 2017, 4(1), 20-25.
- 12 D. Liu, L. He, W. Lei, K. D. Klika, L. Kong and Y. Chen, Multifunctional polymer/porous boron nitride nanosheet membranes for superior trapping emulsified oils and organic molecules, Adv. Mater. Interfaces, 2015, 2(12), 1500228.
- 13 W. Lei, D. Portehault, D. Liu, S. Qin and Y. Chen, Porous boron nitride nanosheets for effective water cleaning, Nat. Commun., 2013, 4, 1777.
- 14 H. Jia, J. Li, Z. Liu, R. Gao, S. Abbas, Y. Fang, C. Yu and C. Tang, Three-dimensional carbon boron nitrides with a broken, hollow, spherical shell for water treatment, RSC Adv., 2016, 6, 78252-78256.
- 15 H. Kobayashi and A. Fukuoka, Hexagonal boron nitride for adsorption of saccharides, J. Phys. Chem. C, 2017, 121(32), 17332-17338.
- 16 S. Yu, X. Wang, W. Yao, J. Wang, Y. Ji, Y. Ai, A. Alsaedi, T. Hayat and X. Wang, Macroscopic, spectroscopic, and theoretical investigation for the interaction of phenol and naphthol on reduced graphene oxide, Environ. Sci. Technol., 2017, 51(6), 3278-3286.
- 17 F. Karlický, E. Otyepková, R. Lo, M. Pitoňák, P. Jurečka, M. Pykal, P. Hobza and M. Otyepka, Adsorption of organic molecules to van der Waals materials: Comparison of fluorographene and fluorographite with graphene and graphite, J. Chem. Theory Comput., 2017, 13(3), 1328-1340.
- 18 J. Roy, S. Ghosh, P. K. Ojha and K. Roy, Predictive quantitative structure-property relationship (QSPR) modeling for adsorption of organic pollutants by carbon nanotubes (CNTs), Environ. Sci.: Nano, 2019, 6(1), 224-247.

- 19 J. Comer, R. Chen, H. Poblete, A. Vergara-Jaque and J. E. Riviere, Predicting adsorption affinities of small molecules on carbon nanotubes using molecular dynamics simulation, ACS Nano, 2015, 9(12), 11761-11774.
- 20 H. Tang, Y. Zhao, S. J. Shan, X. N. Yang, D. M. Liu, F. Y. Cui and B. S. Xing, Wrinkle- and edge-adsorption of aromatic compounds on graphene oxide as revealed by atomic force microscopy, molecular dynamics simulation, and density functional theory, Environ. Sci. Technol., 2018, 52(14), 7689-7697.
- 21 G. Ersan, O. G. Apul and T. Karanfil, Predictive models for adsorption of organic compounds by Graphene nanosheets: comparison with carbon nanotubes, Sci. Total Environ., 2019, 654, 28-34.
- 22 O. G. Apul, Q. Wang, T. Shao, J. R. Rieck and T. Karanfil, Predictive model development for adsorption of aromatic contaminants by multi-walled carbon nanotubes, Environ. Sci. Technol., 2013, 47(5), 2295-2303.
- 23 Y. Wang, J. W. Chen, W. H. Tang, D. M. Xia, Y. Z. Liang and X. H. Li, Modeling adsorption of organic pollutants onto single-walled carbon nanotubes with theoretical molecular descriptors using MLR and SVM algorithms, Chemosphere, 2019, 214, 79-84.
- 24 Y. Wang, J. W. Chen, X. X. Wei, A. J. Hernandez Maldonado and Z. F. Chen, Unveiling adsorption mechanisms of organic pollutants onto carbon nanomaterials by density functional theory computations and linear free energy relationship modeling, Environ. Sci. Technol., 2017, 51(20), 11820-11828.
- 25 Y. Wang, J. Comer, Z. F. Chen, J. W. Chen and J. C. Gumbart, Exploring adsorption of neutral aromatic pollutants onto graphene nanomaterials via molecular dynamics simulations and theoretical linear solvation energy relationships, Environ. Sci.: Nano, 2018, 5(9), 2117-2128.
- 26 B. Delley, An all-electron numerical method for solving the local density functional for polyatomic molecules, J. Chem. Phys., 1990, 92(1), 508-517.
- 27 B. Delley, From molecules to solids with the DMol3 approach, J. Chem. Phys., 2000, 113(18), 7756-7764.
- 28 J. P. Perdew, K. Burke and M. Ernzerhof, Generalized gradient approximation made simple, Phys. Rev. Lett., 1996, 77(18), 3865-3868.
- 29 N. A. Benedek, I. K. Snook, K. Latham and I. Yarovsky, Application of numerical basis sets to hydrogen bonded systems: A density functional theory study, J. Chem. Phys., 2005, 122(14), 144102-144108.
- 30 Y. Inada and H. Orita, Efficiency of numerical basis sets for predicting the binding energies of hydrogen bonded complexes: Evidence of small basis set superposition error compared to Gaussian basis sets, J. Comput. Chem., 2008, 29(2), 225-232.
- 31 P. Liu and J. A. Rodriguez, Catalysts for hydrogen evolution from the [NiFe] hydrogenase to the Ni₂P (001) surface: The importance of ensemble effect, J. Am. Chem. Soc., 2005, 127(42), 14871-14878.
- 32 S. Grimme, Semiempirical GGA-type density functional constructed with a long-range dispersion correction, J. Comput. Chem., 2006, 27(15), 1787-1799.

- 33 H. M. Wang, H. X. Wang, Y. Chen, Y. J. Liu, J. X. Zhao, Q. H. Cai and X. Z. Wang, Phosphorus-doped graphene and (8, 0) carbon nanotube: Structural, electronic, magnetic properties, and chemical reactivity, Appl. Surf. Sci., 2013, 273, 302-309.
- 34 J. Andzelm, C. Kölmel and A. Klamt, Incorporation of solvent effects into the density functional calculations of molecular energies and geometries, J. Chem. Phys., 1995, 103(21), 9312-9320.
- 35 V. Barone and M. Cossi, Quantum calculation of molecular energies and energy gradients in solution by a conductor solvent model, J. Chem. Phys. A, 1998, 102(11), 1995-2001.
- K. Goss, G. Bronner, T. Harner, M. Hertel and T. C. Schmidt, The partition behavior of fluorotelomer alcohols and olefins, Environ. Sci. Technol., 2006, 40(11), 3572-3577.
- 37 M. H. Abraham, P. L. Grellier and R. A. McGill, Determination of olive oil-gas and hexadecane-gas partition coefficients, and calculation of the corresponding olive oilwater and hexadecane-water partition coefficients, J. Chem. Soc., Perkin Trans. 2, 1987, 6, 797-803.
- 38 M. H. Abraham and J. C. McGowan, The use of characteristic volumes to measure cavity terms in reversed phase liquid chromatography, Chromatographia, 1987, 23(4), 243-246.
- 39 M. H. Abraham, G. S. Whiting, R. M. Doherty and W. J. Shuely, Hydrogen bonding. Part 13. A new method for the characterization of GLC stationary phases-The Laffort data set, J. Chem. Soc., Perkin Trans. 2, 1990, 8, 1451-1460.
- 40 M. H. Abraham, G. S. Whiting, R. M. Doherty and W. J. Shuely, Hydrogen bonding. XVI. A new solute solvation parameter, π_2^H , from gas chromatographic J. Chromatogr., 1991, 587(2), 213-228.
- 41 M. H. Abraham, Hydrogen-bonding 31, Construction of a scale of solute effective or summation hydrogen-bond basicity, J. Phys. Org. Chem., 1993, 6(12), 660-684.
- 42 M. H. Abraham, Scales of solute hydrogen-bonding: Their construction and application to physicochemical and biochemical processes, Chem. Soc. Rev., 1993, 22(2), 73-83.
- 43 S. Endo and K. Goss, Predicting partition coefficients of polyfluorinated and organosilicon compounds using polyparameter linear free energy relationships (PP-LFERs), Environ. Sci. Technol., 2014, 48, 2776-2784.
- 44 M. H. Abraham, A. Ibrahim and A. M. Zissimos, Determination of sets of solute descriptors from Chromatogr. chromatographic measurements, 2004, 1037(1-2), 29-47.
- 45 J. A. Platts, M. H. Abraham, D. Butina and A. Hersey, Estimation of molecular linear free energy relationship descriptors by a group contribution approach. 2. Prediction of partition coefficients, J. Chem. Inf. Comput. Sci., 2000, **40**(1), 71–80.
- 46 K. Goss, et al., The Partition behavior of fluorotelomer alcohols and olefins, Environ. Sci. Technol., 2006, 40(11), 3572-3577.
- 47 N. Ulrich, S. Endo, T. N. Brown, N. Watanabe, G. Bronner, M. H. Abraham and K.-U. Goss, UFZ-LSER database v 3.2.1 [Internet], Helmholtz Centre for Environmental Research-UFZ, Leipzig, Germany, 2017.

- 48 Talete srl, Dragon (Software for Molecular Descriptor Calculation) Version 6.0., 2014, http://www.talete.mi.it/.
- 49 P. Gramatica, Principles of QSAR models validation: Internal and external, QSAR Comb. Sci., 2007, 26(5), 694-701.
- J. Li, X. Xiao, X. Xu, J. Lin, Y. Huang, Y. Xue, P. Jin, J. Zou and C. Tang, Activated boron nitride as an effective adsorbent for metal ions and organic pollutants, Sci. Rep., 2013, 3, 3208,
- 51 X. X. Chen and B. L. Chen, Macroscopic and spectroscopic investigations of the adsorption of nitroaromatic compounds on graphene oxide, reduced graphene oxide, and graphene nanosheets, Environ. Sci. Technol., 2015, 49, 6181-6189.
- 52 A. Golbraikh, M. Shen, Z. Y. Xiao, Y. D. Xiao, K. H. Lee and A. Tropsha, Rational selection of training and test sets for the development of validated QSAR models, J. Comput.-Aided Mol. Des., 2003, 17, 241-253.
- 53 T. N. Brown, Predicting hexadecane-air equilibrium partition coefficients (L) using a group contribution approach constructed from high quality data, SAR QSAR Environ. Res., 2014, 25(1), 51-71.
- 54 Y. Liang, R. Xiong, S. I. Sandler and D. M. Di Toro, Quantum chemically estimated Abraham solute parameters using multiple solvent-water partition coefficients and molecular polarizability, Environ. Sci. Technol., 2017, 51(17), 9887-9898.
- 55 C. Robinson and R. E. Schumacker, Interaction effects: centering, variance inflation factor, and interpretation issues, Multiple Linear Regression Viewpoints, 2009, 35, 6-11.
- 56 J. Larsson, J. Gottfries, S. Muresan and A. Backlund,

- ChemGPS-NP: Tuned for navigation in biologically relevant chemical space, J. Nat. Prod., 2007, 70(5), 789-794.
- 57 T. N. G. Borhani, M. Saniedanesh, M. Bagheri and J. S. Lim, OSPR prediction of the hydroxyl radical rate constant of water contaminants, Water Res., 2016, 98, 344-353.
- R. Todeschini and V. Consonni, Handbook of molecular 58 descriptors, Wiley-VCH, Weinheim, Germany, 2000.
- 59 P. De, D. Bhattacharvya and K. Roy, Application of multilayered strategy for variable selection in QSAR modeling of PET and SPECT imaging agents as diagnostic agents for Alzheimer's disease, Struct. Chem., 2019, 30(6), 2429-2445.
- 60 R. Mannhold, G. I. Poda, C. Ostermann and I. V. Tetko, Calculation of molecular lipophilicity: State-of-the-art and comparison of logP methods on more than 96, 000 compounds, J. Pharm. Sci., 2009, 98(3), 861-893.
- 61 E. Papa, P. Pilutti and P. Gramatica, Prediction of PAH mutagenicity in human cells by QSAR classification, SAR OSAR Environ. Res., 2008, 19(1-2), 115-127.
- 62 A. Fernández, R. Rallo and F. Giralt, Prioritization of in silico models and molecular descriptors for the assessment of ready biodegradability, Environ. Res., 2015, 142, 161-168.
- 63 M. Feher and J. M. Schmidt, Property distributions: Differences between drugs, natural products, and molecules from combinatorial chemistry, J. Chem. Inf. Model., 2002, 43(1), 218-227.
- 64 E. Pastorczak and C. Corminboeuf, Perspective: Found in translation: Quantum chemical tools for grasping noncovalent interactions, J. Chem. Phys., 2017, 146(12), 120901.